Quantitative Assessment of Dimensional Evaluation and Artefacts from Filling Materials with CBCT Using Standard Phantom Roots

Xiao Bo CHEN[1,2], Zhe Jun WANG[2], Ya SHEN[2], Andrea ESTEVES[2], He LIU[2,3], Gui Bin HUANG[4], Xiao Yan WANG[4], Lin YUE[4], Markus HAAPASALO[2]

Objective: *To investigate the accuracy of dimensional evaluation and representation of artefacts generated by different gutta-percha (GP) cones with or without sealer with CBCT using a reproducible, standardised phantom root methodology.*
Methods: *The reproducible artificial phantom roots with six root canal sizes from #25 to #50 and 0.04 taper were aligned according to the jaw curvature in a stone model for dimensional measurements. Each root was scanned while empty and filled with four types of filling materials. The specimens were scanned using the CS 9300 3D (Carestream Dental, Rochester, NY, USA) (at two different resolutions), 3D Accuitomo (J Morita, Kyoto, Japan) and NewTom VGi (Verona, Italy) CBCT systems. The hyperdense and hypodense axial slice artefacts from root canal sizes #40, #45 and #50 were recorded.*
Results: *Dimensions were significantly smaller and more accurate with CS 9300/0.09 mm voxel size than with other protocols. The hypodense band was found mostly in the CS 9300 3D system with 0.18 mm voxel size, especially in the buccal-lingual (95%) and coronal (64%) sections. The 3D Accuitomo CBCT system showed the lowest presence of the hypodense band. Areas of both light and dark artefacts were significantly larger in the coronal third than in the apical and middle thirds.*
Conclusion: *Artefacts in the coronal locations and in buccal-lingual sections were more evident in the CS 9300 3D system with a 0.18-mm voxel size.*
Key words: *artefact, CBCT, gutta-percha, measurement, zirconium*
Chin J Dent Res 2023;26(2):83–92; doi: 10.3290/j.cjdr.b4128007

1 Department of Stomatology, Hospital of Tsinghua University, Beijing, P.R. China.
2 Division of Endodontics, Department of Oral Biological & Medical Sciences, Faculty of Dentistry, University of British Columbia, Vancouver, BC, Canada.
3 Department of Stomatology, Affiliated Hospital of Jining Medical University, Jining, Shandong Province, P.R. China.
4 Department of Cariology and Endodontology, Peking University School and Hospital of Stomatology, Beijing, P.R. China.

Corresponding authors: Prof Markus HAAPASALO, Chair, Division of Endodontics, UBC Faculty of Dentistry, 2199 Wesbrook Mall, Vancouver, BC, Canada V6T 1Z3. Tel: 1-604-822-5996; Fax: 1-604-822-3562. Email: markush@dentistry.ubc.ca

Prof Lin YUE, Department of Cariology and Endodontology, Peking University School and Hospital of Stomatology, #22 Zhongguancun South Avenue, Haidian District, Beijing 100081, P.R. China. Tel: 86-10-82195526; Fax: 86-10-62173402. Email: kqlinyue@bjmu.edu.cn

This study was supported by the National Natural Science Foundation of China (U20A20169).

CBCT has been accepted as an essential tool for diagnosis and treatment planning in dentistry, as it permits the construction of 3D images of the targeted teeth and areas[1]. Despite the advances in endodontics produced by CBCT, artefacts have been reported with this tool that can degrade the image quality and mask abnormalities in the presence of high-density obturation materials in the root canals. Worse still, these artefacts cannot be easily avoided[2-4]. Among the possible causes of artefacts, beam hardening is described as the most common. One of the leading causes is the presence of high-density materials within the field of view (FOV); those encountered by endodontists are metal implants, intracanal posts, metallic crowns and amalgam restoration, especially root-filling materials[5]. A reconstructed 3D volume like CBCT represents a reasonable estimation of density within the object at that particular location represented in the particular voxel. Artefacts in the vicinity of highly

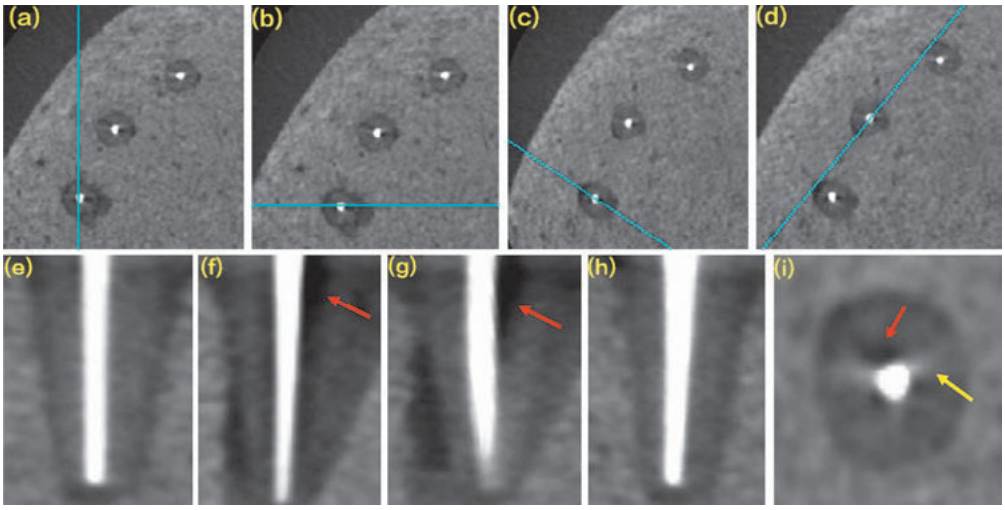

Fig 1 Artefacts in axial and longitudinal sections of EndoSequence GP, #50 in CS 0.18 mm protocol. **(a-d)** Section line for sagittal, coronal, buccal-lingual, and mesiodistal sections in axial views. **(e-h)** Images in sagittal, coronal and buccal-lingual views. **(i)** Axial view. Red arrow, hypodense area; yellow arrow, hyperdense streaks.

dense materials are either caused by beam hardening or by the complete extinction of the beam. Since these materials have extremely high atomic numbers and are highly dense. In this case, zero energy is recorded on the detector "behind" such material.

Artefacts resulting from root-filling material along the long axis of the alveolar bones may result in difficulties with diagnosis[6]. Some previous studies used extracted teeth as the study models to assess the artefacts produced by vertical root fracture[7,8]. Others showed that artefacts might obscure or resemble pathology, and therefore impede accurate diagnosis and subsequent treatment planning[9-14].

Phantom teeth[15] and phantom blocks with pins[5,16] were used in previous studies for artefact assessment. The development of a phantom tooth model with standardised and reproducible root canal morphology can offer a platform to evaluate the accuracy (e.g., area, maximum and minimum diameters) of different obturation materials in the root canal system. So far, few studies have been able to quantify high-density artefacts in CBCT images, especially in standardised phantom roots.

Zinc oxide and barium sulphate in gutta-percha (GP) contribute to the radiopacity of the material. Zirconium is a weak attenuator used in endodontic bioceramic sealers, which may influence the artefacts and the grey values in CBCT images[15]. The grey value has been recognised as the index to assess the density or quality of the material[17]. Despite the good physical, chemical and biological properties of the bioceramic sealer materials[18], properly depicting obturation material in 3D images is challenging. So far, little is known about the impact of obturation materials and bioceramic sealers on CBCT artefacts and accuracy.

The present study aims to develop a reproducible novel artificial phantom root to investigate the artefacts and accuracy of the dimensional evaluation of different root canal filling materials using four CBCT protocols.

Materials and methods

Phantom setup

A reproducible phantom, including a stone model[19] with a standardised straight phantom single root and root canal, was fabricated to measure accuracy and artefacts. To determine the accuracy of dimensional evaluation, the dental stone phantom was fabricated by mixing equal volumes of type III stone plaster (Whip Mix, Louisville, KY, USA) and sawdust, with the shape like the alveolar process of the maxilla. Six sockets were created by arranging MicroAmp tubes (Thermo Fisher Scientific, Waltham, MA, USA), coated with a thin layer of Vaseline, according to the jaw curvature in the phantom model with 6 mm distance between the cervical plane of each root. Equal volumes of epoxy resin (ArtResin, Carrollton, TX, USA) and calcium carbonate (C5929-100G, MilliporeSigma, Burlington, MA, USA) were mixed thoroughly in the tubes, then the filled tubes were vibrated in a VWR Mini Vortexer (Henry Troemner, Thorofare, NJ, USA) for 90 seconds each to eliminate any visible bubbles. Before the resin was set, a 0.04-taper vaseline-coated paper point (Brasseler, Savannah, GA, USA) for one of six different sizes (#25, #30, #35, #40, #45 and #50), was inserted gently in the centre of each resin-filled tube. The top of each tube was covered with a

thin layer of wax to centre the paper points precisely. The paper points were pulled out after the resin was cured, leaving a standard size canal space. Five groups of artificial root fillings, each in six sizes (taper 0.04, size #25 to #50), were prepared: group 1, with no filling; group 2 (GPE), filled with EndoSequence BC GP cones (Brasseler); group 3 (GPV), filled with Vortex GP cones (Dentsply Sirona Endodontics, Tulsa, OK, USA); group 4 (GPEB), filled with EndoSequence BC GP with iRoot SP, root canal sealer (Innovative BioCeramix, Burnaby, BC, Canada); and group 5 (GPVA), filled with Vortex GP with AH Plus sealer (Dentsply DeTrey, Konstanz, Germany). For groups 4 and 5, CBCT scanning was performed after allowing the sealer to set for 72 hours in a water bath at 37^0C.

For the artefact measurements, using the same phantom model, the artificial root canals of three sizes (#40, #45, and #50, taper 0.04) were aligned according to the jaw curvature in sequence (#50 in the posterior region of the dental arch, #45 in the premolar region and #40 in the anterior region) as shown in Fig 1. The artificial root and the real root showed similar radiographic contrast and grey value, as shown by a similar threshold of grey values in Fig 2. Each sample was scanned as unrestored and then restored with four types of root filling materials: EndoSequence BC GP cones only; Vortex GP cones only; EndoSequence BC GP with iRoot SP, injectable root canal sealer; and Vortex GP with AH Plus sealer. The artificial roots for accuracy of dimensional evaluation and artefact measurements were coated with a thin layer of wax (white utility wax strips; Coltene Whaledent, Alstätten, Switzerland) and then placed in the corresponding sockets in the phantom stone model, aligned to the same position for the CBCT scan (Fig 3).

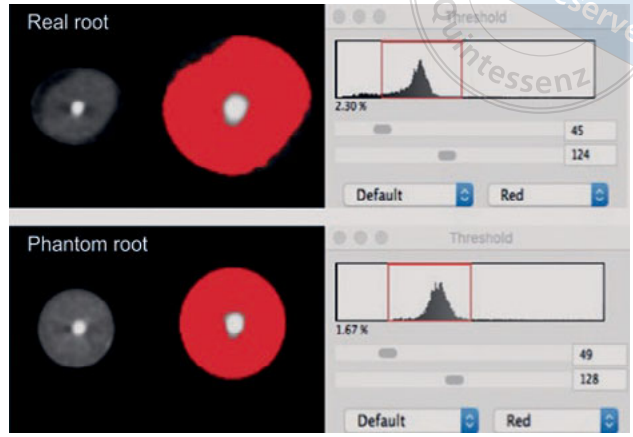

Fig 2 CBCT images of the real root and phantom root scanned by CS 9300 under a voxel size of 0.09 mm. The histograms show nearly identical grey values for both objects.

CBCT image acquisition and processing

The phantom model was positioned on a reproducible platform kept in the same location. The phantom jaw was placed in a round plastic box full of water on the CBCT jig, which was equivalent to a soft tissue surrounding the skull[19]. Images were taken using the following endodontic scanning protocols:

1. CS 9300 3D system (Carestream Dental) with two exposure protocols: 84 kV 5 mA and 90 kV 5 mA. Voxel size and FOV were fixed at 0.09 mm, 5 cm × 5 cm and 0.18 mm, 8 cm × 8 cm (CS0.09, CS0.18);
2. 3D Accuitomo (J. Morita, Kyoto, Japan) with 80 kV 3 mA 0.125 mm, 6 cm × 6 cm (Morita);
3. NewTom VGi (QR SRL, Verona, Italy) with 110 kV 5.2 mA 0.10 mm, 5 cm × 5 cm.

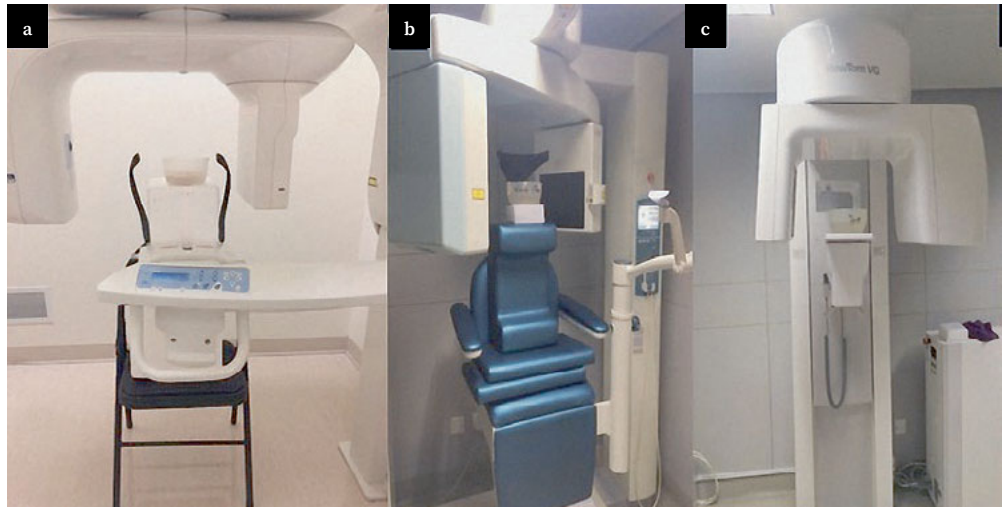

Fig 3 Scanning condition of the phantom. **(a)** CS 9300; **(b)** 3D Accuitomo; **(c)** Newtom VGi).

Table 1 Exposure protocols for each CBCT device.

Parameter	CS9300	CS9300	3D Accuitomo	Newtom VGi
Tube voltage (kV)	90	84	80	110
Tube current (mA)	5	5	3	5.2
Field of view (FOV, mm)	8 × 8	5 × 5	6 × 6	5 × 5
Voxel size (mm)	0.18	0.09	0.125	0.10
Slice thickness (mm)	0.20	0.09	0.125	0.10
Exposure time (s)	19	28	30.8	36
Resolution (1/2*pixels per mm)	2.78	5.56	4	5

Exposure parameters were optimised for the phantom roots. The exposure protocols for each device are listed in Table 1. For the qualitative analysis of the CBCT image, all data were exported as DICOM files and imported into Image J software (version 1.52a, National Institutes of Health, Bethesda, MD, USA) for measurement.

Imaging processing

Dimensional evaluation

A total of 120 volumes were acquired (five groups of six sizes of four exposure protocols). Axial images of roots were selected from three regions: apical (2 mm above the apical end of the root filling/canal), middle (5 mm above the apical end of the root filling/canal) and coronal (8 mm above the apical end of the root filling/canal). Each root adjusted the position according to the axis line from the apex to the central point of the crown plane to make sure the cross-section was perpendicular to the long axis of the root while measuring. For each region, five images at the slice thickness intervals were selected (segment slice and two adjacent slices in both apical and coronal directions). The diameters of phantom root fillings at the three measurement locations (2 mm, 5 mm, 8 mm above the apical end of the root filling) were measured using a digital Vernier caliper before being placed in each phantom root canal, which was used as a "ground truth". A total of 450 images were selected for each exposure protocol (15 slices with five groups, six sizes), with no filling group as the baseline for control. The resulting images were set to 8-bit colour depth, saved with a black background in TIFF format and imported into ImageJ software.

All the axial images with fillings were measured with ImageJ, using a wand (tracing tool) to segment the target automatically with the same fixed tolerance and threshold regions. Area and the maximum and minimum diameter of axial canal images were all calculated by the ImageJ software algorithm. The threshold tool and fixed region of interest (ROI) tool were both used to represent the area.

Artefact measurement

The artefact pixel intensity value ranges were established for the hyperdense zone (light) and hypodense (dark) artefacts for each protocol, respectively. Threshold tools and fixed ROI tools were used manually, along with standardised segmentation of the area for light and dark artefacts for each axial section. Within the ROIs, areas of light and dark artefacts were measured according to the grey value threshold using the software. Both light and dark artefacts were seldom observed in the apical part of sizes #25, #30 and #35. Thus, axial slice artefacts from root canal sizes #40, #45 and #50 were recorded. A total of 225 axial images in TIFF format were selected for each exposure protocol (15 slices with five groups, three sizes). Longitudinal images were acquired from four directions (Figs 1a to d), all passing through the centre of the tooth. As such, a set of four longitudinal images for each group were obtained as follows: one in sagittal view and one in coronal views (Figs 1e and f), one in buccal-lingual (B-L) view, and one in mesiodistal (M-D) view (Figs 1g and h). The hypodense band in a total of 60 longitudinal images in TIFF format was selected for each exposure protocol (slices of four direwctions with five groups, three sizes). The score for the hypodense band was recorded in all acquired longitudinal images with scores given according to the absence (0) or presence (1) of the dark band. Continuous and linear change of grey value was analysed in longitudinal sections using plot profile tools and surface profile tools in ImageJ. A total of 900 (225*4) axial images and 240 (60*4) longitudinal images were analysed twice over a 2-week period under the same display condition.

All CBCT scanning, evaluation and measurement were performed by the same three experienced radiologists and endodontists trained in CBCT diagnostic applications.

Statistical analysis

SPSS (version 25; IBM, Armonk, NY, USA) was used for statistical tests. The level of statistical significance was set at $P < 0.05$. The data were analysed statistically using a

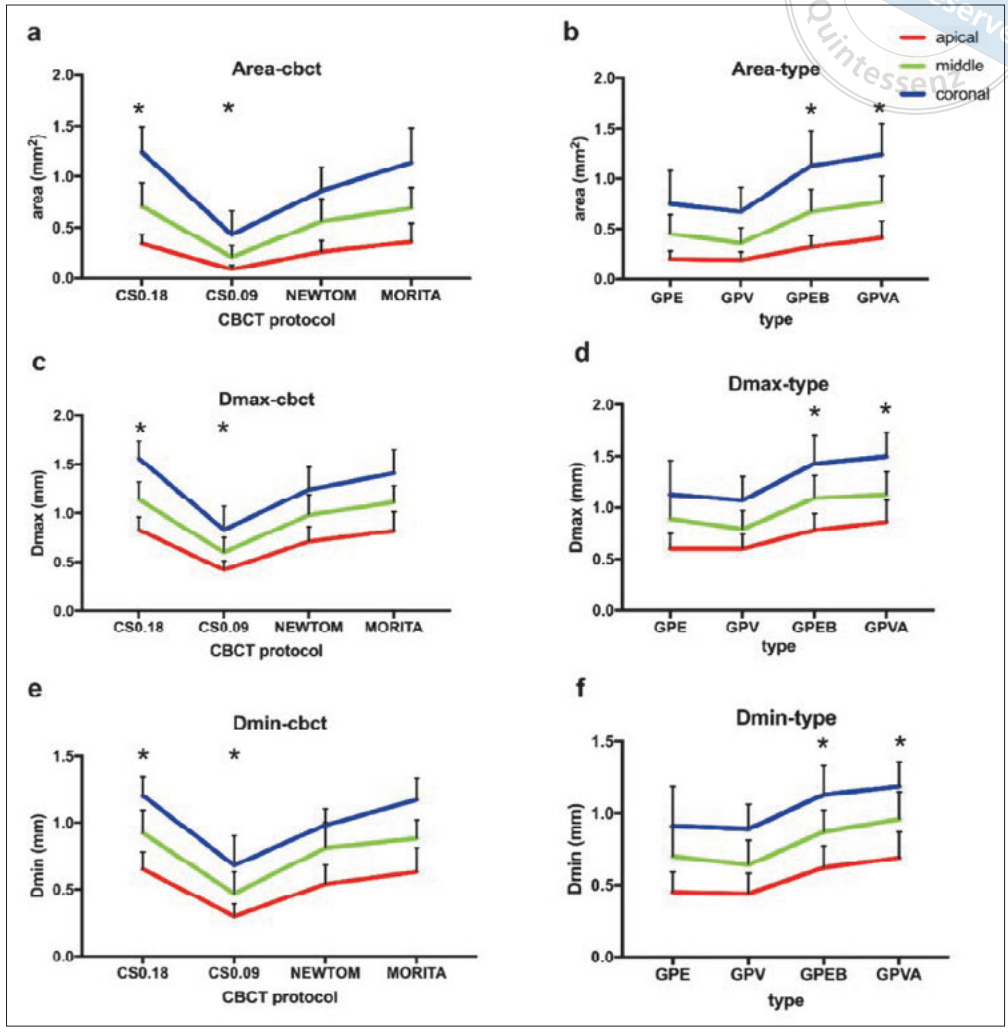

Fig 4 Comparison of areas **(a and b)**, maximum diameters **(c and d)** and minimum diameters **(e and f)** among CBCT protocols and filling types in size #30. *Statistically significant difference compared with the other groups of the same line, $P < 0.05$.

one-way analysis of variance followed by a Tukey test and multiple linear regression. A Kappa test was used to assess interobserver and intraobserver agreement for the three observers. A chi-squared test was applied to compare the average presence of artefacts evaluated by the three observers (two experienced endodontists and one experienced oral radiologist) for different slice orientations.

Results

The interobserver and intraobserver agreement ranged from 0.706 to 0.838 (substantial) for reading of the longitudinal sections.

Dimensional evaluation

Both the areas and diameters of root fillings with CS 9300/0.09 mm voxel size were significantly smaller than for the other three CBCT protocols as shown in Fig 4 ($P < 0.001$) in all root filling sizes. The maximum/minimum diameters of root filling of #30 canal fillings in CS 9300, for example, were 0.42 + 0.09 mm/0.30 + 0.08 mm (2 mm above the apical end of the root filling); 0.60 + 0.15 mm /0.47 + 0.15 mm in the middle part (5 mm above the apical end of the root filling); and 0.83 + 0.22 mm/0.68 + 0.20 mm in the coronal part (8 mm above the apical end of the root filling), depending on the CBCT protocol (Table 2). CS 9300/0.18 mm voxel size produced the largest filling area and diameters, especially when compared to CS 9300 using a voxel size of 0.09 mm ($P < 0.05$).

Taking root canal filling size #30 as an example, images of groups of EndoSequence BC GP with BC iRoot SP sealer (GPEB) and Vortex GP with AH Plus sealer (GPVA) both showed significantly larger areas (Fig 4; $P < 0.001$), and bigger maximum (Fig 4; $P < 0.001$) and minimum diameters (Fig 4; $P < 0.001$) than those of the

Table 2 Maximum and minimum diameters of root filling.

w	Location	#25 Dmax/Dmin (mm)	#30 Dmax/Dmin (mm)	#35 Dmax/Dmin (mm)	#40 Dmax/Dmin (mm)	#45 Dmax/Dmin (mm)	#50 Dmax/Dmin (mm)
CS 0.18	Apical	0.79 + 0.11/ 0.56 + 0.11	0.83 + 0.13/ 0.65 + 0.13	0.97 + 0.16/ 0.71 + 0.15	1.06 + 0.18/ 0.79 + 0.15	1.18 + 0.15/ 0.85 + 0.11	1.24 + 0.13/ 0.87 + 0.10
	Middle	1.07 + 0.12/ 0.79 + 0.11	1.14 + 0.18/ 0.92 + 0.17	1.23 + 0.19/ 1.01 + 0.10	1.31 + 0.10/ 1.10 + 0.14	1.41 + 0.12/ 1.13 + 0.13	1.54 + 0.15/ 1.19 + 0.14
	Coronal	1.40 + 0.16/ 1.09 + 0.15	1.56 + 0.16/ 1.20 + 0.14	1.59 + 0.16/ 1.25 + 0.14	1.63 + 0.18/ 1.32 + 0.12	1.71 + 0.19/ 1.32 + 0.18	1.77 + 0.19/ 1.36 + 0.19
*CS 0.09	Apical	0.38 + 0.10/ 0.27 + 0.09	0.42 + 0.09/ 0.30 + 0.08	0.45 + 0.12/ 0.33 + 0.10	0.56 + 0.12/ 0.45 + 0.11	0.65 + 0.11/ 0.56 + 0.14	0.79 + 0.13/ 0.67 + 0.12
	Middle	0.57 + 0.17/ 0.42 + 0.12	0.60 + 0.15/ 0.47 + 0.15	0.63 + 0.15/ 0.53 + 0.13	0.79 + 0.11/ 0.65 + 0.10	0.85 + 0.10/ 0.72 + 0.11	0.90 + 0.11/ 0.76 + 0.12
	Coronal	0.78 + 0.17/ 0.60 + 0.16	0.83 + 0.22/ 0.68 + 0.20	0.89 + 0.21/ 0.71 + 0.81	1.03 + 0.13/ 0.87 + 0.10	1.11 + 0.16/ 0.96 + 0.11	1.15 + 0.17/ 0.99 + 0.15
NewTom	Apical	0.71+ 0.14/ 0.54 + 0.17	0.76 + 0.15/ 0.57 + 0.14	0.81 + 0.18/ 0.62 + 0.16	0.91 + 0.25/ 0.72 + 0.20	0.95 + 0.26/ 0.80 + 0.20	1.05 + 0.22/ 0.79 + 0.13
	Middle	1/02 + 0.21/ 0.75 + 0.12	0.98 + 0.21/ 0.81 + 0.14	1.02 + 0.12/ 0.86 + 0.17	1.14 + 0.22/ 0.90 + 0.19	1.17 + 0.21/ 0.99 + 0.12	1.25 + 0.24/ 1.02 + 0.15
	Coronal	1.26 + 0.24/ 0.97 + 0.15	1.24 + 0.23/ 0.98 + 0.12	1.39 + 0.27/ 1.06 + 0.21	1.40 + 0.30/ 1.12 + 0.21	1.49 + 0.18/ 1.18 + 0.22	1.52 + 0.17/ 1.22 + 0.12
Morita	Apical	0.82 + 0.13/ 0.63 + 0.16	0.86 + 0.19/ 0.65 + 0.18	0.86 + 0.19/ 0.67 + 0.23	0.86 + 0.19/ 0.67+0.18	0.86 + 0.19/ 0.71+0.14	0.86 + 0.19/ 0.75+0.13
	Middle	1.07 + 0.20/ 0.79 + 0.18	1.11 + 0.17/ 0.88 + 0.14	1.11 + 0.17/ 0.89 + 0.16	1.11 + 0.17/ 0.87 + 0.17	1.11 + 0.17/ 0.94 + 0.15	1.11 + 0.17/ 0.97 + 0.16
	Coronal	1.35 + 0.19/ 1.08 + 0.15	1.41 + 0.24/ 1.17 + 0.16	1.41 + 0.24/ 1.15 + 0.21	1.41 + 0.24/ 1.14 + 0.15	1.41 + 0.24/ 1.19 + 0.17	1.41 + 0.24/ 1.21 + 0.13

*Statistically significant difference compared with the other groups in the same location, $P < 0.05$.

Table 3 Presence of hypodense halo in longitude sections.

CBCT protocol	Sagittal	Coronal	Buccal-lingual	Mesiodistal
CS 0.18	0.25	0.64^{ab}	0.95^{ab}	0.31^{abc}
CS 0.09	0.19	0.50^{c}	0.61	0.06^{a}
NewTom	0.08	0.08^{a}	0.36^{a}	0.00^{b}
Morita	0.00	0.00^{bc}	0.36^{b}	0.00^{c}

^{a,b,c}Different superscript letters in each line indicate a significant difference ($P < 0.05$).

GPE and GPV groups in the apical, middle and coronal parts of the roots. The smallest area and maximum diameter were found in the GPV group ($P < 0.001$). When comparing the GPV group to the GPE group, there was no significant difference in the minimum diameter. The GPVA group showed the largest areas in all filling groups ($P < 0.001$).

Artefact measurement

Artefacts appeared like streaks and hypodense areas (Fig 1). In a total of 192 CBCT images, hypodense areas were found mostly in the CS 9300 3D system with a voxel size of 0.18 mm in all four longitudinal sections: 64% in coronal, 25% in sagittal, 95% in buccal-lingual and 31% in mesiodistal sections (Table 3), followed by the CS 9300 system with a voxel size of 0.09 mm. The 3D Accuitomo CBCT system showed a low presence of artefacts, and only in buccal-lingual sections of size #40 (anterior zone). Hypodense artefacts were observed significantly more often in coronal and buccal-lingual sections, but less in sagittal and mesiodistal sections in all four protocols.

The roots filled with Vortex GP (GPV group) exhibited the smallest light areas (hyperdense artefacts) in all four CBCT protocols and in all three locations ($P < 0.001$). EndoSequence GP with BC sealer (GPEB group) and Vortex GP with AH Plus sealer (GPVA group) showed the largest light areas. With the CS 9300 3D

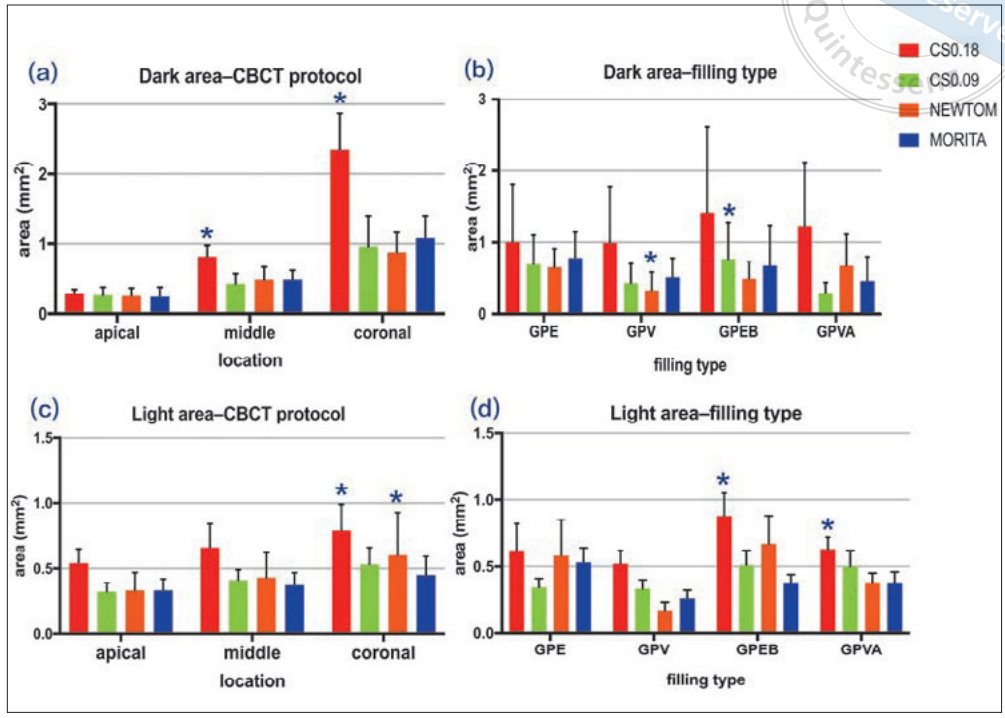

Fig 5 Comparison of areas (mm^2) of light and dark artefacts among different CBCT **(a and c)** and root filling protocols **(b and d)** in the #50 group. *Statistically significant difference compared with the other groups of the same colour bar, $P < 0.05$.

system with a voxel size of 0.18 mm, the light areas in the GPEB group were significantly larger than for the GPVA group ($P = 0.009$). Measurements of the dark areas (hypodense artefacts) were performed only in the size #50 group. The GPV group showed the smallest dark areas with NewTom protocols, and the GPEB group had the largest dark areas with the CS 0.09 protocol. When using CS 9300/0.18mm and Morita protocols, dark areas of the four root-filling groups showed no significant differences. With the CS 9300 3D system with a voxel size of 0.18 mm, light and dark area artefacts were both significantly larger than for the other three CBCT protocols in apical, middle and coronal locations ($P < 0.001$). Both light and dark areas were significantly larger in the coronal part than in the apical and middle part ($P < 0.001$) in all four CBCT protocols and all four types of filling materials. Figure 5 shows the performance of the size #50 group. The dark areas of the middle location were significantly larger than those of the apical location for the CS 0.18 mm, NewTom, and Morita CBCT protocols ($P < 0.001$, $P < 0.001$, $P = 0.003$, respectively).

In the longitudinal sections exhibiting hypodense haloes, the plot profile analysis demonstrated an obvious decline in grey value adjacent to the GP in the coronal section, approaching zero in the nearest portion, when compared to the control group with no filling material (Fig 6); however, in the sagittal section, a slight increase in grey value was detected for the GP close to the root wall.

Discussion

This study used an artificial phantom root to quantitatively evaluate the dimensional evaluation and metal (high-density) artefacts generated by different filling materials. The advantage of artificial roots created in this study is that they are reproducible and with the same size (length and width) similar to real teeth. The model is easy to build and enables reliable comparison of parameters from CBCT images taken using different protocols. Furthermore, the material selected for the artificial roots has a similar radiopacity to real roots (Fig 2).

Besides the widely used AH Plus sealer and traditional GP cones, where barium and zinc are the main contributors to radiopacity, the newly introduced bioceramic sealer and GP were also investigated. New root canal obturation materials (e.g., Endosequence GP cones and sealer) with lower radiopacity profiles[20] and improved CBCT software algorithms are expected to minimise imaging artefacts. EndoSequence BC Sealer was investigated[14] and no significant difference was detected in fracture diagnostics between the zirconium-based filling material and traditional ones. In the present study, although the areas of artefacts in

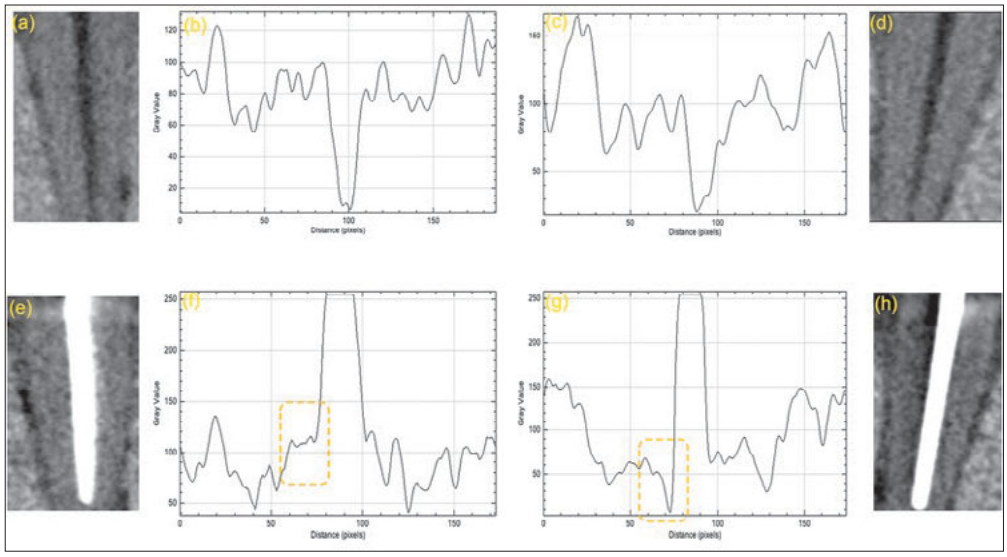

Fig 6 Views and plot profile analysis of size #50 with no filling **(a-d)** and filled with EndoSequence GP **(e-h)** in the CS 0.09 mm protocol in sagittal **(a, b, e, f)** and coronal **(c, d, g, h)** views, demonstrating an evident decline in grey value adjacent to the GP in the coronal section, but no reduction in the sagittal section.

roots filled with zirconium-based fillings appeared to be smaller than those in roots filled with GP Vortex and AH Plus sealer, no significant difference was detected.

The thresholding method[15,21] was applied and a fixed ROI was used in the present study. The present study developed a reproducible methodology for characterising artefacts generated from GP with or without sealers and to quantitatively assess artefacts based on phantom roots.

It has been reported that identical tissues may appear to present different greyscale intensity values depending upon their position relative to other tissues in the irradiated field[17]. To minimise this, each root was kept in the same position in the same model during each scan. A previous study claimed that if the grey value is too high, artefacts may occur and compromise measurement accuracy, especially in the border area of the images[17]. In fact, it is not the grey value that causes these effects; it is the density and atomic number of the real object that causes beam hardening or even beam extinction. It is important to remember that radiography always measures absorption, which translates into the physical parameter "density". In other words, reconstructed CBCT images represent a reasonable estimation of density within the object at that location represented in the particular voxel. Artefacts in the vicinity of highly dense (extremely high atomic numbers) materials are mostly caused by beam hardening. In this context, this might also explain why more artefacts were observed in the buccolingual dimension and in parts of thicker root-filling material, as shown in Table 3. Following the explanation above, this is simply due to more (non-linear) absorption in these regions/directions and thus more incorrect redistribution of the recorded values, i.e., more prominent artefacts.

The CBCT protocol was shown to be the most reliable predictor of both hyperdense and hypodense artefacts by multiple regression. The hypodense (dark) area was most obvious in the CS9300 3D system, especially with a voxel size of 0.18 mm. In B-L sections, it even reached an incidence of 0.95 in the dark band, while dark areas larger than 2 mm^2 were seen in the coronal location. Artificial lines in the oblique directions resulting from root-filling material may resemble root fractures. These hypodense artefacts were not observed with Accuitomo previously[2,22], which is consistent with the findings of the present study. The 3D Accuitomo CBCT system only showed a 36% incidence of artefacts in B-L sections (#40 size: anterior region), whereas the incidence for the other three sections was all zero.

Both light and dark areas were largest in the coronal parts of the canals, especially for the dark area in the coronal location with CS 0.18, which is consistent with previous studies[2,15]. The greater light artefact area in the coronal third was associated with the larger volume of root fillings in this third. For the middle and apical thirds of the canal, fewer light artefacts were observed because of the smaller volume of root fillings. This may explain the difficulty in reading and segmentation in sizes #40 and #45 of the root canal fillings for the dark artefacts. This finding is also in line with the notion of strengthening minimal instrumentation in modern endodontics to save dentine by reducing instrumentation sizes[23], leading to lighter artefacts.

Artefacts may have a significant impact on diagnosis, planning and follow-up[24]. An image-reading approach[25]

suggests that a map-reading strategy of viewing sequential axial slices resolved the problem[26]. Longitudinal images were obtained and analysed according to this protocol in the present study. The surface plot of grey value in Fig 6 demonstrated an evident decline adjacent to GP in this apparently hypodense band. B-L and coronal sections showed the highest incidence of the hypodense band even with the 3D Accuitomo, indicating that careful interpretation is essential to avoid an incorrect diagnosis of fracture lines or under-obturation[2]. In the back-projection process, which is no more than a highly simplified inversion of the true physical projection process, the recorded energy is "smeared back" from the detector pixels along the ray paths towards the source, and in such cases incorrect (relatively too high) energies are distributed in the reconstruction volume. This causes dark (hyperdense) bands that are always along the back-projection lines. Extinction would cause hyperdense (light) stripes along those lines; however, a posteriori "correction" of the reconstructed volume as implemented by manufacturers may often alter the colour of the stripes. This makes it difficult to correct, as the information on the true density cannot be derived from the projections as they are the only source used for CBCT scans. Thus, the present study described the performance of artefacts induced by root canal fillings rather than revealing the internal cause of artefacts. Such information could be derived from evaluating thousands of existing computed tomography or CBCT scans and using this information in learning systems, such as artificial intelligence.

Conclusion

CBCT showed acceptable accuracy of measurement of filling material dimensions. More artefacts were detected in the CS 9300 3D system with a voxel size of 0.18 mm in the coronal location and in the B-L section.

Conflicts of interest

The authors declare no conflicts of interest related to this study.

Author contribution

Dr Xiao Bo CHEN contributed to the conceptualisation of the study and drafted the manuscript; Drs Zhe Jun WANG, Ya SHEN, Andrea ESTEVES and He LIU contributed to the analysis and interpretation of data; Gui Bin HUANG contributed to drafting the manuscript and finalising the article; Dr Xiao Yan WANG contributed to drafting the manuscript; Drs Lin YUE and Markus HAAPASALO contributed to the conception and design of the study and the supervision of the project.

(Received Sep 21, 2022; accepted Jan 31, 2023)

References

1. Liang YH, Jiang L, Gao XJ, Shemesh H, Wesselink PR, Wu MK. Detection and measurement of artificial periapical lesions by cone-beam computed tomography. Int Endod J 2014;47:332–338.
2. Vasconcelos KF, Nicolielo LF, Nascimento MC, et al. Artefact expression associated with several cone-beam computed tomographic machines when imaging root filled teeth. Int Endod J 2015;48:994–1000.
3. Panjnoush M, Kheirandish Y, Kashani PM, Fakhar HB, Younesi F, Mallahi M. Effect of exposure parameters on metal artefacts in cone beam computed tomography. J Dent (Tehran) 2016;13:143–150.
4. Pinto MGO, Rabelo KA, Sousa Melo SL, et al. Influence of exposure parameters on the detection of simulated root fractures in the presence of various intracanal materials. Int Endod J 2017;50:586–594.
5. Codari M, de Faria Vasconcelos K, Ferreira Pinheiro Nicolielo L, Haiter Neto F, Jacobs R. Quantitative evaluation of metal artefacts using different CBCT devices, high-density materials and field of views. Clin Oral Implants Res 2017; 28:1509–1514.
6. Iikubo M, Nishioka T, Okura S, et al. Influence of voxel size and scan field of view on fracture-like artefacts from gutta-percha obturated endodontically treated teeth on cone-beam computed tomography images. Oral Surg Oral Med Oral Pathol Oral Radiol 2016;122:631–637.
7. da Silveira PF, Vizzotto MB, Liedke GS, da Silveira HLD, Montagner F, da Silveira HED. Detection of vertical root fractures by conventional radiographic examination and cone beam computed tomography: An in vitro analysis. Dent Traumatol 2013; 29:41–46.
8. Brady E, Mannocci F, Brown J, Wilson R, Patel S. A comparison of cone beam computed tomography and periapical radiography for the detection of vertical root fractures in nonendodontically treated teeth. Int Endod J 2014;47:735–746.
9. Patel S, Brady E, Wilson R, Brown J, Mannocci F. The detection of vertical root fractures in root filled teeth with periapical radiographs and CBCT scans. Int Endod J 2013;46:1140–1152.
10. Moudi E, Haghanifar S, Madani Z, Alhavaz A, Bijani A, Bagheri M. Assessment of vertical root fracture using cone-beam computed tomography. Imaging Sci Dent 2014;44:37–41.
11. Jones D, Mannocci F, Andiappan M, Brown J, Patel S. The effect of alteration of the exposure parameters of a cone-beam computed tomographic scan on the diagnosis of simulated horizontal root fractures. J Endod 2015;41:520–525.
12. Katkar R, Steffy DD, Noujeim M, Deahl ST 2nd, Geha H. The effect of milliamperage, number of basis images, and export slice thickness on contrast-to-noise ratio and detection of mandibular canal on cone beam computed tomography scans: An in vitro study. Oral Surg Oral Med Oral Pathol Oral Radiol 2016;122:646–653.
13. Menezes RF, Araújo NC, Santa Rosa JMC, et al. Detection of vertical root fractures in endodontically treated teeth in the absence and in the presence of metal post by cone-beam computed tomography. BMC Oral Health 2016;16:48.

14. Fox A, Basrani B, Lam EWN. The performance of a zirconium-based root filling material with artifact reduction properties in the detection of artificially induced root fractures using cone-beam computed tomographic imaging. J Endod 2018;44:828–833.
15. Fox A, Basrani B, Kishen A, Lam EWN. A novel method for characterizing beam hardening artefacts in cone-beam computed tomographic Images. J Endod 2018;44:869–874.
16. Martins LAC, Queiroz PM, Nejaim Y, de Faria Vasconcelos K, Groppo FC, Haiter-Neto F. Evaluation of metal artefacts for two CBCT devices with a new dental arch phantom. Dentomaxillofac Radiol 2020;49:20190385.
17. Katsumata A, Hirukawa A, Okumura S, et al. Effects of image artefacts on gray-value density in limited-volume cone-beam computerized tomography. Oral Surg Oral Med Oral Pathol Oral Radiol Endod 2007;104:829–836.
18. Wang ZJ. Bioceramic materials in endodontics. Endodontic Topics 2015;32:3–30.
19. Brito-Júnior M, Santos LA, Faria-e-Silva AL, Pereira RD, Sousa-Neto MD. Ex vivo evaluation of artefacts mimicking fracture lines on cone-beam computed tomography produced by different root canal sealers. Int Endod J 2014;47:26–31.
20. Pawar AM, Pawar S, Kfir A, Pawar M, Kokate S. Push-out bond strength of root fillings made with C-Point and BC sealer versus gutta-percha and AH Plus after the instrumentation of oval canals with the Self-Adjusting File versus WaveOne Int Endod J 2016;49:374–381.
21. Rabelo KA, Cavalcanti YW, de Oliveira Pinto MG, et al. Quantitative assessment of image artefacts from root filling materials on CBCT scans made using several exposure parameters. Imaging Sci Dent 2017;47:189–197.
22. Makeeva IM, Byakova SF, Novozhilova NE, et al. Detection of artificially induced vertical root fractures of different widths by cone beam computed tomography in vitro and in vivo. Int Endod J 2016;49:980–989.
23. Wolters WJ, Duncan HF, Tomson PL, et al. Minimally invasive endodontics: a new diagnostic system for assessing pulpitis and subsequent treatment needs. Int Endod J 2017;50:825–829.
24. Kim JH, Arita ES, Pinheiro LR, Yoshimoto M, Watanabe PCA, Cortes ARG. Computed tomographic artefacts in maxillofacial surgery. J Craniofac Surg 2018;29:e78–e80.
25. Bueno MR, Estrela C, De Figueiredo JA, Azevedo BC. Map-reading strategy to diagnose root perforations near metallic intracanal posts by using cone beam computed tomography. J Endod 2011;37:85–90.
26. Hekmatian E, Karbasi Kheir M, Fathollahzade H, Sheikhi M. Detection of vertical root fractures using cone-beam computed tomography in the presence and absence of gutta-percha. Scientific World Journal 2018;2018:1920946.